



**CHALMERS**

---

# CPL

*Chalmers Publication Library*

Institutional Repository of  
Chalmers University of Technology  
<http://publications.lib.chalmers.se>

---

Copyright 2011 Society of Photo-Optical Instrumentation Engineers. One print or electronic copy may be made for personal use only. Systematic electronic or print reproduction and distribution, duplication of any material in this paper for a fee or for commercial purposes, or modification of the content of the paper are prohibited.

<http://dx.doi.org/10.1117/12.881247>

# Tuneable VCSEL aiming for the application in interconnects and short haul systems

Christian Gierl<sup>a</sup>, Karolina Zogal<sup>a</sup>, Sandro Jatta<sup>a</sup>, Hooman A. Davani<sup>a</sup>, Franko Küppers<sup>a</sup>,  
 Peter Meissner<sup>a</sup>,  
 Tobias Gründl<sup>b</sup>, Christian Grasse<sup>b</sup>, Markus-Christian Amann<sup>b</sup>,  
 Aidan Daly<sup>c</sup>, Brian Corbett<sup>c</sup>,  
 Benjamin Kögel<sup>d</sup>, Åsa Haglund<sup>d</sup>, Johan Gustavsson<sup>d</sup>, Petter Westbergh<sup>d</sup>, Anders Larsson<sup>d</sup>,  
 Pierluigi Debernardi<sup>e</sup>,  
 Markus Ortsiefer<sup>f</sup>

<sup>a</sup>Technische Universität Darmstadt, Merkstrasse 25, Darmstadt, Germany

<sup>b</sup>Walter Schottky Institut, Am Coulombwall 3, Garching, Germany

<sup>c</sup>Tyndall National Institute, Lee Maltings, Cork, Ireland

<sup>d</sup>Chalmers University of Technology, Gothenburg, Sweden

<sup>e</sup>Istituto di Elettronica e di Ingegneria dell'Informazione e delle Telecomunicazioni, Corso  
 Duca degli Abruzzi 24, Torino, Italy

<sup>f</sup>VERTILAS GmbH, Lichtenbergstrasse 8, Garching, Germany

## ABSTRACT

Widely tuneable vertical cavity surface emitting lasers (VCSEL) are of high interest for optical communications, gas spectroscopy and fiber-Bragg-grating measurements. In this paper we present tuneable VCSEL operating at wavelengths around 850 nm and 1550 nm with tuning ranges up to 20 nm and 76 nm, respectively. The first versions of VCSEL operating at 1550 nm with 76 nm tuning range and an output power of 1.3 mW were not designed for high speed modulation, but for applications where only stable continuous tuning is essential (e.g. gas sensing). The next step was the design of non-tuneable VCSEL showing high speed modulation frequencies of 10 GHz with side mode suppression ratios beyond 50 dB. The latest version of these devices show record output powers of 6.7 mW at 20 °C and 3 mW at 80 °C. The emphasis of our present and future work lies on the combination of both technologies. The tuneable VCSEL operating in the 850 nm-region reaches a modulation bandwidth of 5.5 GHz with an output power of 0.8 mW.

**Keywords:** Tuneable VCSEL, High-Speed, High-Power, Wide Tunability, Telecommunication, Optical Interconnects, Short Haul Systems

## 1. INTRODUCTION

Today, broadband communication has become a very important resource for our quick growing society. During the information era, communication has become a basic need. Every year, the number of internet users increases rapidly and with it the requirements for today's telecommunication networks. The increasing supply of services, such as real-time high definition video streaming and peer to peer file exchange require low delay and high capacity access networks. Given standards like digital subscriber line (DSL - phone) or hybrid fiber coax (HFC - cable) will not be able to fulfill the future requirements on broadband access networks, for they are already reaching their capacity limits. Even the most recent very high speed digital subscriber line (VDSL2) is limited to 100 MBit/s in up- and downstream direction.<sup>1</sup> Thus the near future is asking for a new infrastructure which fulfills the requirements of future demands.

A very promising candidate is the passive optical network (PON) which allows to provide high performance and

---

Further author information: (Send correspondence to Christian Gierl)

Christian Gierl: E-mail:Gierl@ont.tu-darmstadt.de, Telephone: +49 6151 16 4418

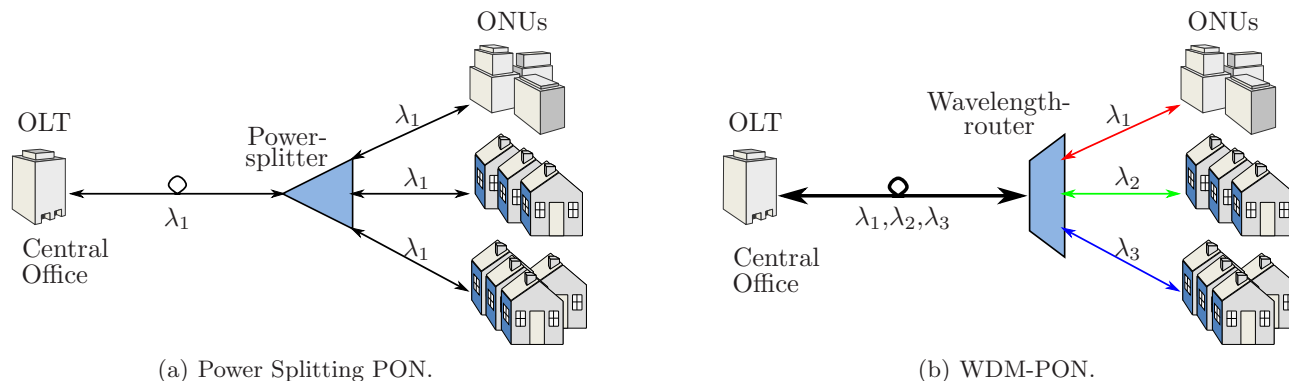


Figure 1. In a Power splitting PON, the power of the downstream signal is splitted via a power splitter to the different ONUs (a). In a WDM-PON a wavelength router separates the different wavelength of the downstream to the appropriate users (b), which is a physical point to point connection.

low delay services. In a PON the connection between optical line terminal (OLT) at the service providers central office and the optical network units (ONU) near the end users is based only on passive optical components. Thus no electrical power is needed within the feeder network. Furthermore PONs have two significant advantages as compared to the given standards like VDSL2. First, it exploits the very high channel capacity of optical fibres enabling access to broadband intensive services. The lower attenuation per length in optical fibre networks compared to electrical networks is the second advantage.

There mainly exist two different PON architectures. Wavelength division multiplexing (WDM) PONs (e.g. DWDM-PONs, channel spacings of 100 GHz in the range of 1528.77 nm to 1563.86 nm, ITU G.692<sup>2</sup>) and today's time-division multiple access (TDMA) PONs like Ethernet PON (EPON, IEEE 802.3ah<sup>3</sup>) and gigabit PON (GPON, ITU-T G.984<sup>4</sup>). However, the latter cannot keep up with future requirements regarding bandwidth, attainable reach and allowable power budget. This approach uses a passive power splitting unit to split the optical power in the feeder fibre equally to the ONUs (Fig. 1a). However, this concept limits the flexibility for assigning different bandwidths (wavelength) to different ONUs since every ONU has to communicate at the same data rate. A WDM-PON<sup>5</sup> overcomes these limitations and offers a higher optical bandwidth per ONU, low splitting losses and thus a higher link reach as opposed to EPON and GPON networks.<sup>6</sup> WDM-PON access networks use wavelength selective filters<sup>7</sup> instead of power splitters for separating the information for the different ONUs (Fig. 1b). This technique allows the OLT to address each ONU by selecting the appropriate wavelength thus allowing different data rates and privacy. All of the WDM-PON approaches are trying to solve one of the main challenges which is to provide cost effective light sources at the OLT and the ONUs. We will focus on the approach using a photonic integrated circuit at the OLT and a tunable vertical cavity emitting diode laser (VCSEL) at the ONU. Each ONU uses an identical tunable VCSEL which is able to tune to any given wavelength of the channel grid. This attempt is called "colorless" ONU. Whereas the OLT is equipped with an array of lasers combined in a photonic integrated circuit (PIC).<sup>8</sup> Tunable VCSEL are highly desirable components for WDM-PON networks for several reasons. In order to supply for example a 100-channel WDM system, one would need 100 different distributed feedback lasers with fixed wavelength. This matter leads to several disadvantages. The laser manufacturers need to introduce expensive selection processes for supplying the ONUs with lasers of the appropriate wavelength. Moreover, the network operators need to stock many different lasers and keep inventories of spare parts for each laser wavelength in the event transmitters fail in the field and need to be replaced. A tunable VCSEL would be able to compensate all of these disadvantages. Only one "colorless" ONU would be needed which reduces the capital as well as operational expenditures.

Another application for tunable VCSEL are short distance communication networks. Such networks are used in high-end computing, switching and storage systems. They can be used e.g. as optical interconnects in distributed shared memory machines (DSM).<sup>9</sup> The CPU performance has increased rapidly following Moore's law.<sup>10</sup> Whereas the bandwidth of the interconnects between the processors and the memory has not increased this fast. This gap in performance becomes a significant problem in massively parallel processing (MPP) systems.<sup>11</sup> Electrical interconnects suffer from attenuation, crosstalk and reflections inside the electrical signal lines which becomes

even worse for higher bus speeds. Thus optical interconnects using WDM are very attractive for MPP or DSM systems. They enable a significant increase in bandwidth as well as more complex interconnect topologies.<sup>11</sup> Many different concepts for tunable laser sources have been investigated in the past decades.<sup>13-15</sup> Tunability describes the ability of a single mode laser to change its operating wavelength via an external control parameter. The tuning range of such a laser can be defined by the given requirements of the application. These requirements could be side mode suppression ratio (SMSR), output power, linewidth or relative intensity noise (RIN), which must not go below or above a certain limit or keep constant over the tuning range. In telecommunication, the tuning range should cover the entire C-band (1529 nm to 1565 nm) or L-band (1565 nm to 1610 nm) or even both. A SMSR > 30 dB and data rates of about 10 GBit/s are recommended. In short distance data communication networks a tuning range of  $\geq 30$  nm in the range of 820 nm to 880 nm and a modulation bandwidth  $\geq 10$  GBit/s are desirable.

## 2. TUNABILITY OF VCSEL

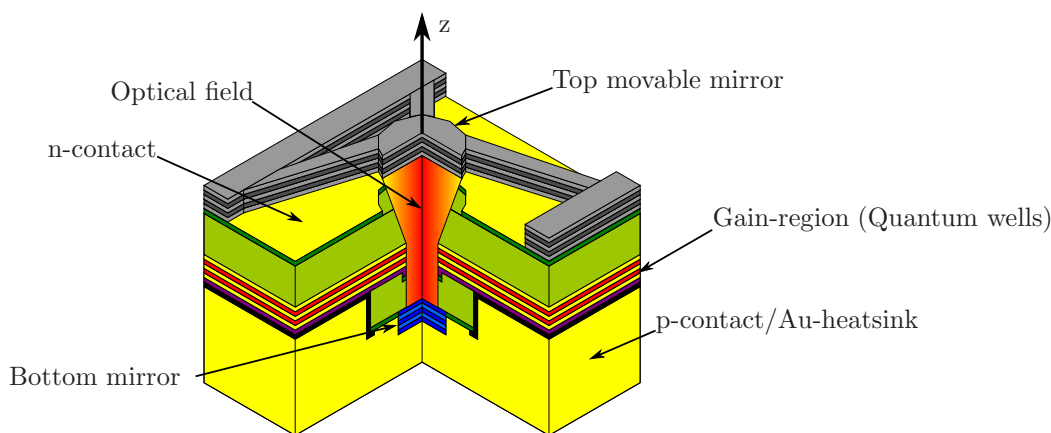


Figure 2. Cross-section of a MEMS tunable VCSEL. The bottom and the curved top mirror form an optical resonator. The optical field inside the resonator is amplified in the gain region. The top mirror can be moved along the z-axis which changes the cavity length.

The basic physics of a tunable VCSEL can be best explained with the principle of Fabry-Pérot lasers. Such a laser consists of two parallel mirrors with an active gain material for light amplification in between. This can be an electrically pumped semiconductor whose parallel crystal surfaces form a resonator consisting of two plain mirrors (the semiconductor air interface has a sufficient reflectivity of  $\approx 30\%$ ). After each reflection, the light passes the electrically pumped gain medium and is amplified. A stable laser mode inside the cavity is only possible if the circulating wave in between two crystal surfaces superimposes itself in-phase (a standing wave inside the resonator):

$$L = nL' = m \frac{\lambda_m}{2} \quad (1)$$

where  $L'$  is the geometrical cavity length,  $n$  the effective refraction index,  $m$  an integer and  $\lambda_m$  the emitted wavelength. The main mechanism for tuning a laser is to change the effective optical cavity length  $L$  and thus the wavelength  $\lambda$ . There exist three parameters for changing the emitted wavelength. The first one is the temperature of the device (thermo optical effect). An increase of the temperature  $T$  leads to a change of the refractive index ( $n(T)$ ) and thus to an increase of the wavelength  $\lambda$ . The wavelength change over temperature is typically 0.09 to 0.12 nm/ $^{\circ}\text{C}$ <sup>12</sup> and limited to a continuous tuning range of about 7 nm for standard VCSEL (see measurement results in section 5). The second one is the injection current, which changes the carrier density  $C$  inside the cavity and therewith the refractive index ( $n(C)$ ) index  $n$ . As the device heats up for higher currents, this effect is limited to several nm, too. The third one is to change the cavity length mechanically. In this paper we will focus on micro-electro-mechanical (MEMS) tunable VCSEL (see Fig. 2). This concept enables record tuning ranges  $> 70$  nm.<sup>15</sup>

### 3. BASIC PRINCIPLE OF A MEMS TUNABLE VCSEL

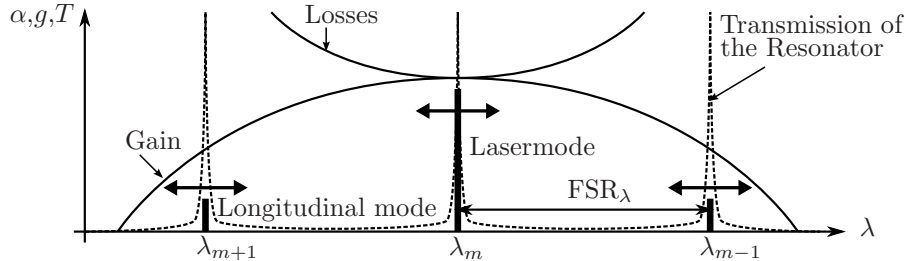


Figure 3. The selectivity of the Fabry-Pérot resonator of a short cavity VCSEL allows only one longitudinal mode ( $\lambda_m$ ) to lase. The adjacent longitudinal modes ( $\lambda_{m+1}, \lambda_{m-1}$ ) underlie too high losses.

A MEMS tunable VCSEL mainly consists of an electrically pumped active region embedded between two distributed bragg reflectors (DBR). They are based on the principle of interference and enable very high reflectivities ( $> 99\%$ ). These reflectivities are needed since the active region is quite short as compared to edge emitting diode lasers which reduces the gain during one pass through the active medium significantly. One can separate the tunable VCSEL into two main parts. The first part mainly consists of the bottom mirror and the active gain region. This part is called half-VCSEL, because the second mirror is missing. Our devices use a curved movable mirror membrane which is suspended on four flexible beams as top mirror.<sup>15</sup> An implemented conductive layer allows thermal heating of the membrane and thus an expansion of the suspension beams. This leads to an increase of the air gap length (see fig. 7). The curved top mirror and the flat bottom mirror of the half-VCSEL are forming a plane-concave Fabry-Pérot cavity. This type of cavity is much more insensitive to tilt angles between the two mirrors as compared to cavities consisting of two plane mirrors.<sup>16</sup> Furthermore we will see that this approach can be used to further increase the SMSR and to guarantee stable optical properties over the whole tuning range, too. The MEMS tunable VCSEL devices presented in this paper can be described as optical oscillators with resonant wavelengths defined by equation (1). The standing waves are the longitudinal eigenmodes of the optical resonator. The free spectral range (FSR) between two longitudinal modes is given by

$$FSR_\lambda = \lambda_m - \lambda_{m+1} \approx \frac{\lambda^2}{2L}. \quad (2)$$

This equation illustrates one advantage of VCSEL as a tunable laser source. In comparison to edge emitting lasers, the resonator length of typically  $L = 10\lambda$  is quite short and leads to a  $FSR_\lambda \approx \lambda/20 \approx 80\text{ nm}$  at a wavelength of  $\lambda = 1550\text{ nm}$ . Because of the limited amplification bandwidth  $g$  of the gain medium, the losses  $\alpha$  of the passive resonator and the large spectral distance of the longitudinal modes (Transmission  $T$  of the resonator), only one longitudinal mode has a sufficient amplification for lasing (a schematic view of  $\alpha, g$  and  $T$  is given in fig. 3). This intrinsic single mode behaviour allows a continuous tuning of the wavelength. Another advantage is the tuning efficiency. A change in the distance of the two resonator mirrors of  $\Delta L$  leads to a linear shift of the wavelength  $\Delta\lambda$  with

$$\Delta\lambda = \Delta L \cdot \frac{2}{m} \quad (3)$$

whereas  $m$  is the order of the longitudinal mode. In our example with a typical resonator length of  $L = 10\lambda$  one gets  $m = 20$  and therewith  $\Delta\lambda = 0.1\Delta L$ . Whereas a typical edge emitter with  $L = 450\lambda$  has a tuning efficiency of only  $\Delta\lambda/\Delta L \approx 0.005$  which is twenty times smaller. The consequence is, that a reduction of the resonator length effects an increase of the tuning efficiency. Never the less a tuning over the whole  $FSR$  requires a change of the resonator length of  $\Delta L = \lambda/2 \approx 780\text{ nm}$ , which is independent of the resonator length.

#### 3.1 Resonator geometry and Gaussian modes

In section 3 we introduced a one dimensional model for Fabry-Pérot resonators and calculated its one dimensional longitudinal modes. To describe their three dimensional field distributions inside a plane-concave resonator, this

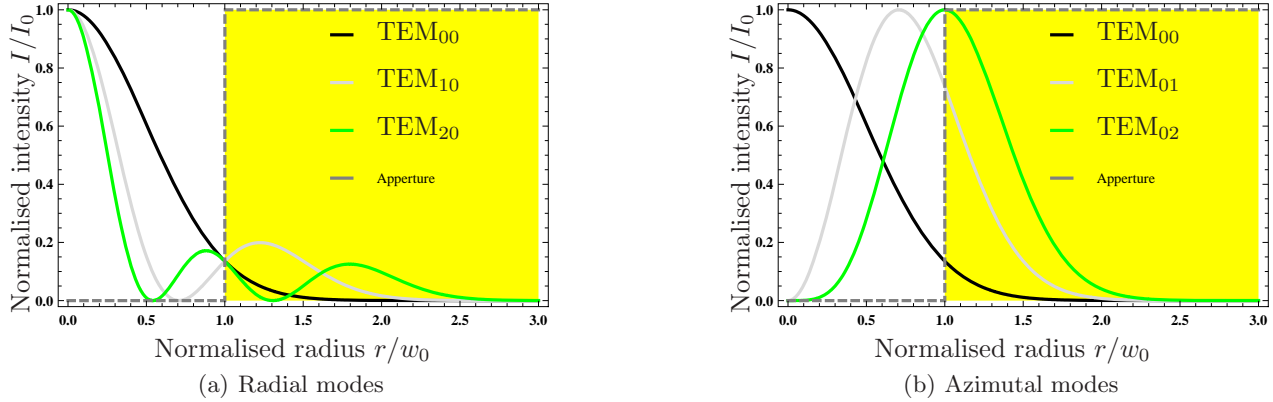


Figure 4. Cross section view of the intensity distribution for radial (a) and azimuthal Gauss-Laguerre-modes  $TEM_{pl}$  (b). The implementation of an aperture inside the resonator (shaded area) allows to increase the losses for higher order modes which leads to a significant increase of the SMSR.

model needs to be extended. The three dimensional electrical field distribution of the longitudinal modes inside the resonator can be approximated by the radial symmetric Gaussian beam equation (in cylindrical coordinates)

$$E(r, z) = E_0 \frac{w_0}{w(z)} \cdot \exp\left(-\frac{r^2}{w(z)^2}\right). \quad (4)$$

This equation is completely defined with the beam waist  $w_0 = w(z = 0)$  of the Gaussian beam and the Rayleigh length  $z_0 = \pi w_0^2 / \lambda$ . The Gaussian beam diverges in  $z$ -direction at which  $w(z)$  defines the beam radius along the propagation axis  $z$ . The phasefront  $R(z)$  of the Gaussian beam transforms from a plane wave at  $z = 0$  into a spherical wave for  $z \rightarrow \infty$  with

$$w(z) = w_0 \sqrt{1 + \left(\frac{z}{z_0}\right)^2} \quad ; \quad R(z) = z \left(1 + \left(\frac{z_0}{z}\right)^2\right) \quad (5)$$

Thus the Gaussian mode is completely defined by the radius of curvature ( $RoC$ ) of the top movable mirror membrane and the cavity length  $L$  (in  $z$ -direction, see Fig. 2), so that the phasefronts of the Gaussian mode coincide with the mirror geometries. This circumstance causes a plane phasefront at the bottom mirror of the VCSEL with a given beam waist of

$$w_0 = \sqrt{\frac{\lambda}{\pi}} \sqrt{L(RoC - L)}. \quad (6)$$

In fact, a rotation symmetric resonator is not restricted to the longitudinal Gaussian modes. Transversal higher order modes fulfill the boundary conditions of the resonator as well. These modes can be described as  $TEM_{pl}$  modes with the radial and azimuthal order  $p$  and  $l$ , respectively. In fact, the intensity distributions inside the complex VCSEL device can not completely be described with  $TEM_{pl}$ -modes but with hybrid modes with longitudinal field components.<sup>18</sup> But the Gaussian beam theory can be used as a good approximation. The intensity profile for the  $TEM_{pl}$  modes can be calculated with the Gauss-Laguerre-polynomes  $L_p^l(t)$  (in polar coordinates  $(r, \phi)$ ) as follows:

$$I_{pl}(r, \phi) = I_0 \cdot t^l \cdot (L_p^l(t))^2 \cdot \cos^2(l\phi) \cdot e^{-t} \quad \text{with} \quad t = 2r^2/w_0^2. \quad (7)$$

For higher order modes, the intensity distribution spreads in radial direction. A cross section view of the higher order radial (a) as well as azimuthal modes (b) is shown in Fig. 4 (the intensity distributions are symmetric to the Intensity-axis). This fact allows us to increase the losses for higher order modes with the implementation of an aperture inside the VCSEL structure (coloured area in Fig. 4). Thus a significant increase of the SMSR is

possible. In a plane concave resonator each  $TEM_{pl}$  mode has its characteristic resonance frequency

$$\nu_{plq} = \frac{c}{2L} \left( q + \frac{2p+l+1}{\pi} \arccos \left( \sqrt{1 - L/RoC} \right) \right) \quad (8)$$

with longitudinal order  $q$ . The measurement of the emission spectrum allows to identify the lateral modes and thus the SMSR as will be shown in section 5.

### 3.2 Lateral and longitudinal confinement factor

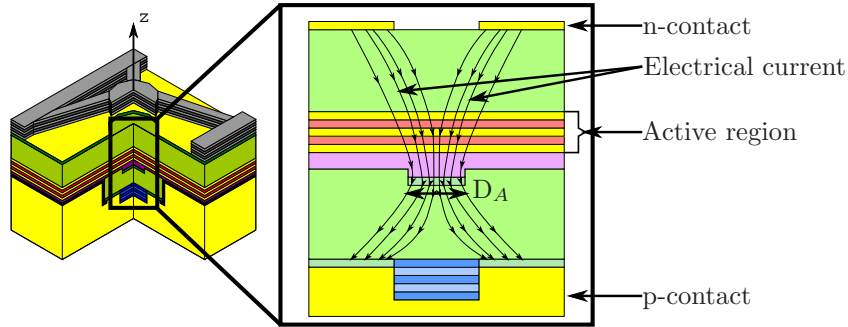


Figure 5. The current flowing from the n- to the p-contact is confined to the diameter  $D_A$  of the integrated aperture. The active region is electrically pumped only within this area which leads to a spatial confinement of the gain.

The size of the integrated aperture is chosen to be in the range of the beam waist of the fundamental Gauss-mode. As illustrated in fig. 4, the fundamental mode is nearly not effected by the aperture, whereas the higher order modes have a larger overlap between the intensity distribution and the apperture. The basic principle behind the aperture is to confine the current flowing through the device to a defined diameter  $D_A$  (see Fig. 5). Since the gain profile is directly correlated with the current density, the overlap between the lateral gain  $g(r, \phi)$  and the transversal intensity distribution  $I_{pl}(r, \phi) \propto |E_{pl}(r, \phi)|^2$  for a certain mode  $p, l$  can be described by the lateral confinement factor

$$\Gamma_{xy} = \frac{\int |E_{pl}(r, \phi)|^2 g(r, \phi) r dr d\phi}{\int |E_{pl}(r, \phi)|^2 r dr d\phi}. \quad (9)$$

Considering a constant gain profile limited by the integrated aperture, one can calculate that  $\Gamma_{xy}(E_{00}) > \Gamma_{xy}(E_{pl})$  for  $p$  or  $l > 0$ . Thus the fundamental Gaussian mode has a higher gain as compared to higher order transversal modes leading to an increase of the SMSR. With the longitudinal confinement factor  $\Gamma_z$  which quantizes the overlap between the longitudinal intensity distribution of a given mode and the active gain region

$$\Gamma_z = \frac{\int_{d_{gain}} |E_{pl}(z)|^2 dz}{\int_L |E_{pl}(z)|^2 dz}, \quad (10)$$

one can calculate the effective gain  $\langle g \rangle = \Gamma g = \Gamma_{xy} \Gamma_z g$  for each resonator mode. The longitudinal confinement factor  $\Gamma_z$  compares the thickness of the active region  $d_{gain}$  with the resonator length  $L$ . Thus equation 10 can be written as<sup>19</sup>

$$\Gamma_z = \frac{d_{gain}}{L} \cdot \Gamma_r \quad \text{with} \quad \Gamma_r = 1 + \cos(2k_z \Delta z) \frac{\sin(k_z d_{gain})}{k_z d_{gain}}. \quad (11)$$

The relative confinement factor  $\Gamma_r$  describes the overlap between the standing wave and the active region inside the VCSEL cavity, with the wavenumber  $k_z$  and the relative shift  $\Delta z$  of the nodes and antinodes of the standing wave while changing the cavity length with the movable membrane. If an antinode of  $|E(z)|^2$  overlaps with the

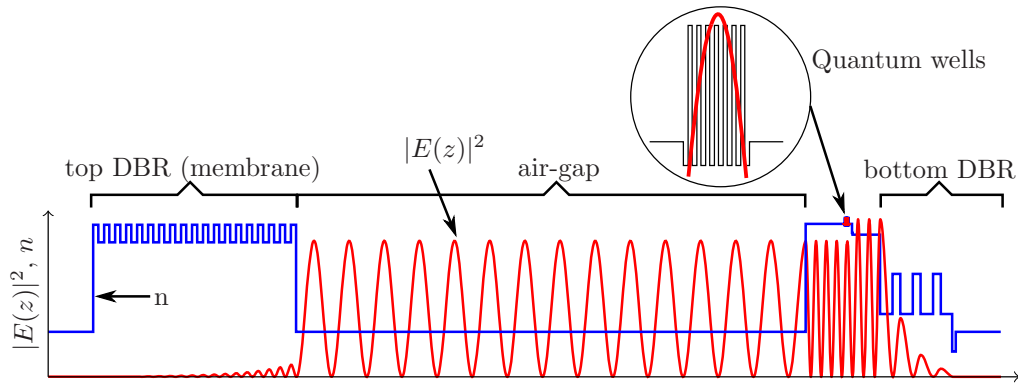


Figure 6. Simulation of the longitudinal 1D intensity distribution ( $|E(z)|^2$ ) in a long-wavelength tunable VCSEL. The refractive index profile  $n(z)$  is defined by the layer composition of the VCSEL. The blow-up shows that  $|E(z)|^2$  has an antinode inside the gain region (quantum wells)

active region,  $\Gamma_r$  has a maximum value of two. On the other hand, if a node coincides with the active region,  $\Gamma_r$  becomes zero. Thus the tunable VCSEL needs to be designed in a way that an antinode overlaps with the active region for a maximum effective gain. The one dimensional longitudinal intensity distribution has been simulated considering every single layer and its refraction index of a given tunable VCSEL-design (via Matrix-Transfer-Method<sup>20</sup> implemented with Matlab-software\*). Fig. 6 shows that the intensity distribution has an antinode inside the gain region for an air-gap length of  $11 \mu\text{m}$ .

#### 4. TECHNOLOGY AND FABRICATION

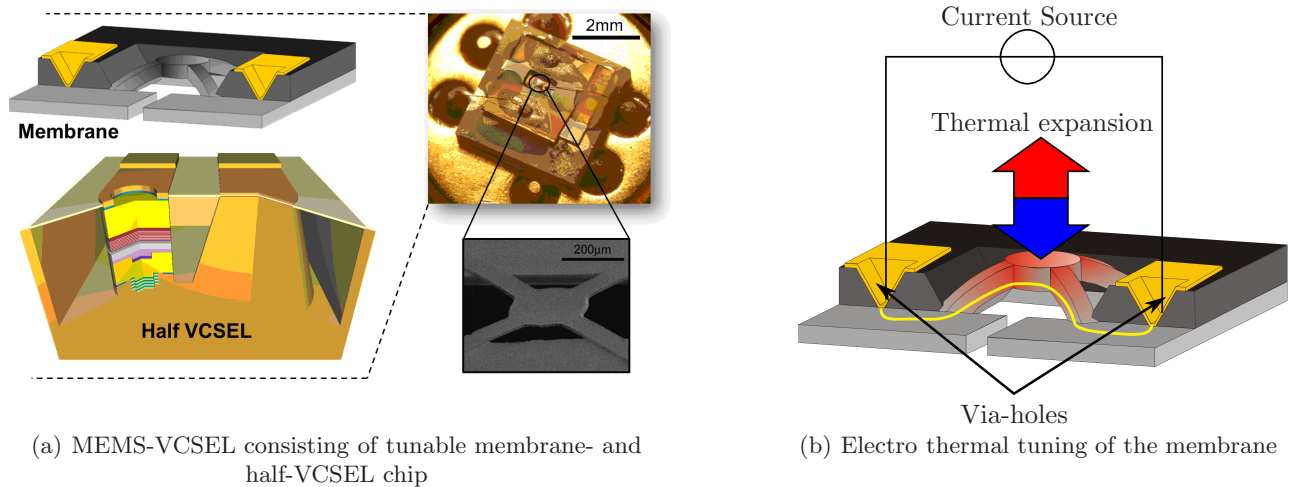
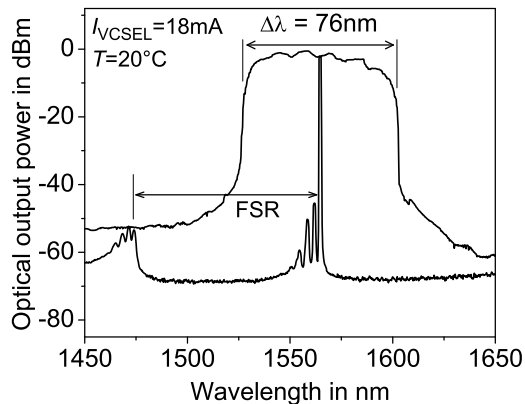


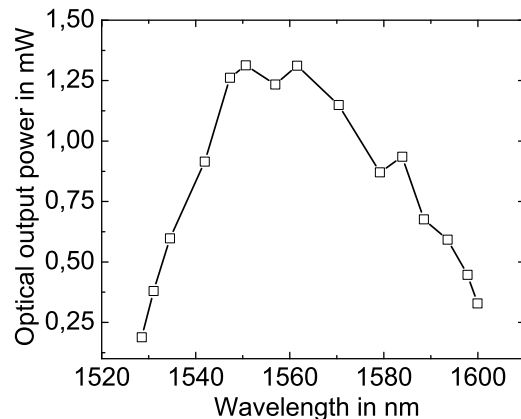
Figure 7. Realization of the MEMS-VCSEL concept with a movable top mirror membrane which can be electro-thermally actuated. Its deflection is directly correlated to the emission wavelength of the VCSEL device and can be controlled via a heating current flowing through the membrane.

Micro-electro-mechanical-system (MEMS) technology is very promising in respect to the achievement of stable spectral properties over a large tuning range ( $> 70 \text{ nm}$ ).<sup>15</sup> By use of a curved mirror (with a defined RoC) the fundamental mode of the VCSEL can be supported. Essential for this approach is the coincidence of the phasefront of the optical beam with the curvature of the membrane. The included length of air-gap can be varied by using electro thermal actuation thus the cavity resonance can be tuned to longer wavelengths. The MEMS-DBR is realised in two different material systems: semiconductive and dielectric. The semiconductor

\*Trademark of MathWorks



(a) Optical emission spectrum for a fixed tuning current and tuning envelope



(b) Output power over tuning range

Figure 8. Measurement results for a long wavelength VCSEL with a dielectric DBR membrane. A record tuning range of 76 nm has been achieved.

DBR consists of MBE-grown GaAs/Al<sub>0.85</sub>Ga<sub>0.15</sub> as  $\lambda/4$ -thick layers with a refractive index contrast of 0.39. The inclusion of an Indium content up to 5% at the upper part of the mirror induces a stress gradient, which then results in a defined membrane deflection. The semiconductor DBR layers are doped with Si during the epitaxy process to enable electrical conductivity for electro thermal heating of the membrane. Two via-holes are etched into the GaAs-substrate to allow electrical connection to a current source. While heating the membrane, the deflection remains stable and there is no tilt of the membrane which would cause losses in the resonator owing to the symmetric four beam design (see Fig. 7). The dielectric DBRs consist of alternating SiO/SiN layers deposited on a GaAs substrate. Each layer has an optical thickness of  $\lambda/4$ . The advantage of this material composition is the high difference of the refractive index ( $\Delta n = 0.5$ ) resulting in fewer layers and a higher stop bandwidth compared with a semiconductor mirror with the same reflectivity. The deposition of the dielectric layers is performed with plasma enhanced chemical vapour deposition (PECVD). The concave bending of the dielectric mirror membrane is realized with a mechanical stress inside the layers by changing the process parameters of the PECVD. Because dielectric material does not conduct current, one can not use the semiconductor actuation scheme without any modifications. To facilitate material heating, an additional conductive metal (Ni) layer has been designed. The idea basing on two-chip configuration is presented in Fig. 7. The mirror-membrane can be actively aligned for a maximum output power and fixed in this position with UV-curable adhesive.

## 4.1 Long wavelength VCSEL

The first versions of long wavelength VCSEL were not designed for high speed modulation, but for applications where only stable continuous tuning is essential. A very short summary of those results is given in section 4.1.1. The next step was the design of non tunable VCSEL showing high speed modulation (see section 4.1.2). The emphasis of our present and future work lies on the combination of both technologies.

### 4.1.1 Tunable VCSEL

Using the two-chip technology we were able to design and fabricate several tunable electrically pumped long wavelength VCSEL. The first version used GaAs/AlGaAs DBR membranes and showed a tuning range of 28 nm and an output power of 1.7 mW.<sup>22</sup> Using an additional anti reflection coating on the half-VCSEL surface, the tuning range could be increased to 58 nm and an output power of 1.8 mW.<sup>23</sup> The best tuning range with still an output power of 1.3 mW was achieved using a broadband dielectric DBR (SiN/SiO). The tuning range of this device (76 nm) was limited by the FSR of the cavity (see fig. 8).<sup>15</sup>

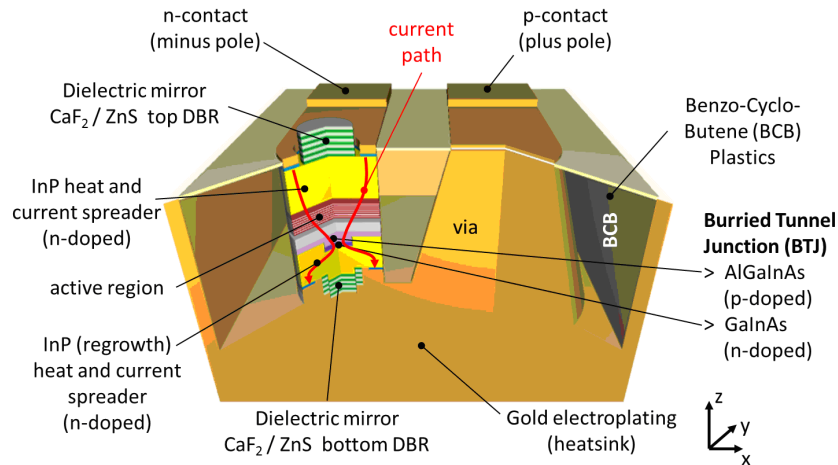


Figure 9. Cross-section of a high-speed 1.55  $\mu\text{m}$  InP-based BTJ VCSEL

#### 4.1.2 Non tunable high speed VCSEL

The single-mode high speed VCSEL operating in the 1.55  $\mu\text{m}$  wavelength range is based on InP-semiconductor cavity with a buried tunnel junction (BTJ). Figure 9 shows the cross-section of the half VCSEL. The active region consists of seven highly compressively strained AlGaInAs quantum wells (QW) with a thickness of 6 nm which are separated by 7 nm thick lattice matched AlGaInAs barriers. This compressive strain increases the differential gain of the active region, which is essential for high speed properties.<sup>21</sup> The active region is embedded between two thick InP layers (see "InP n-cladding" and "InP regrowth" in fig. 9). By lowering the doping level of the n-InP overgrowth, the parasitic capacitance of the space charge region is reduced. This leads to strongly reduced device parasitics,<sup>24</sup> which is essential to gain access to  $> 10$  GBit/s modulation frequencies. Current confinement and thus a sufficient high current density in the active region is achieved by implementing a BTJ.<sup>25, 27</sup> The BTJ consists of two highly doped layers, namely AlGaInAs (p-doped,  $1.5 \cdot 10^{20} \text{ cm}^{-3}$ ) and GaInAs (highly n-doped  $1.5 \cdot 10^{20} \text{ cm}^{-3}$ ). The dielectric bottom DBR consists of evaporated  $\text{AlF}_3/\text{ZnS}$  with gold coating and an electroplated substrate (serving as heatsink). The advantage of these materials is the high refractive index contrast  $\Delta n \approx 1$ , therefore only 3.5 pairs are needed to reach a desired reflectivity beyond 99%. The next advantage is that a reduction of the DBR thickness is possible. This is important due to the better heat management of the whole device. However, the thickness of the DBR is not critical in respect to the electrical resistance, since the given design uses intracavity current injection. That means that the current does not have to flow through all the DBR layers to reach the active region. The next important technological advancement is a shrinkage of the contact pad area and the inclusion of Benzo-Cyclo-Butene (BCB) with a low dielectric constant of 2.6, which is intended to reduce the parasitic contact pad capacitances and hence enable high speed operation.

#### 4.2 Short wavelength VCSEL

Starting from the bottom GaAs-substrate, the half-VCSEL consists of an n-type GaAs contact layer above the n-contact (Ni/Ge/Au). The bottom DBR consists of 36.5 pairs of n-doped AlGaAs with a maximum reflectivity of 99.9%, a gain region consisting of three GaAs QW and a top p-region. An Al-rich layer has been set just above the QW. This layer can be selectively oxidized and define simultaneously a current and gain aperture. Additionally, the semiconductor-air interface is covered with a  $\lambda/4$  anti-reflection coating. To be able to supply the VCSEL with a high-frequency signal a 1.3 mm long microstrip line connects the VCSEL to ground-signal-ground (G-S-G) pads (fig. 10). A 6  $\mu\text{m}$  thick layer of BCB separates the transmission line from the ground plane. Etching small mesa structures and filling the etched regions with BCB significantly reduces the parasitic capacitance. This enables modulation frequencies  $> 5$  GHz. The top concave mirror membrane of the VCSEL consists of AlGa(In)As layers grown by molecular beam epitaxy on an undoped GaAs substrate. The high-index

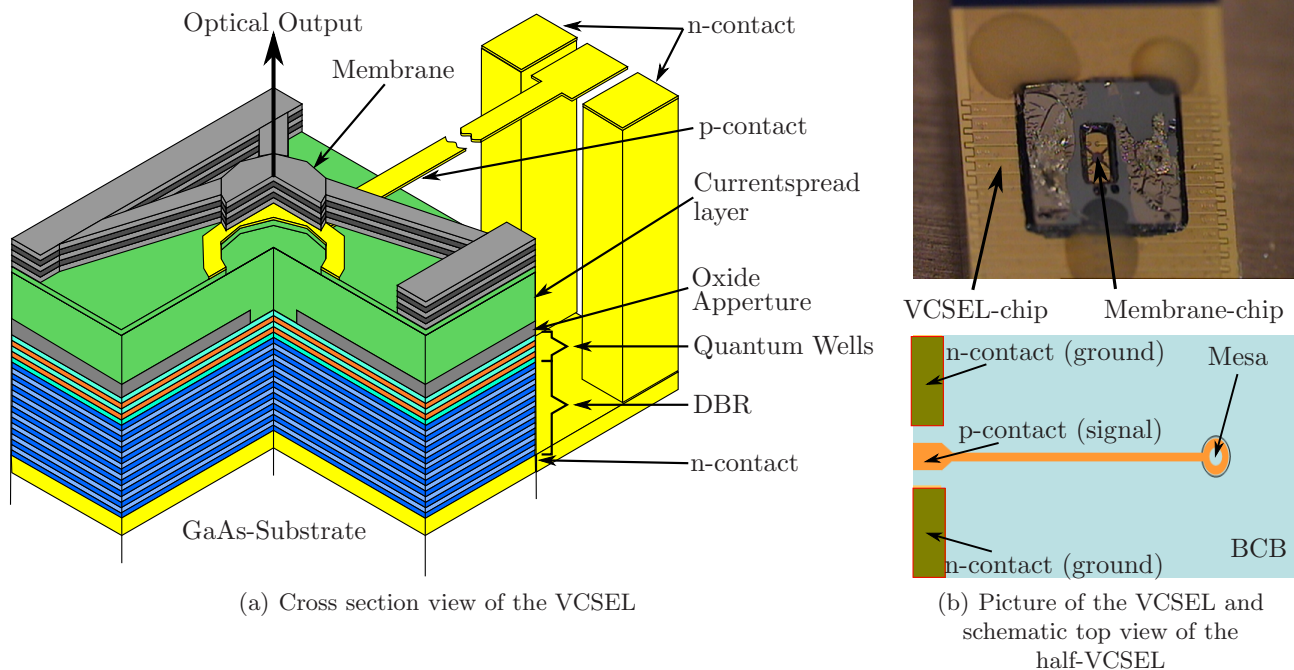


Figure 10. Cross-section of a high-speed 850 nm GaAs-based VCSEL with integrated oxide aperture. The area around the mesa structure is filled with BCB which reduces the parasitic capacitance. The top picture in (b) shows a membrane chip assembled with the half-VCSEL.

layers have an aluminium-content of 14% and the low-index layers are composed of  $\text{Al}_{0.85}\text{GaAs}$ . This results in a refractive index difference of about 0.4. To achieve a reflection of 99.8%, 22.5 pairs are required. Due to difficulties in the fabrication process, eight of 22.5 pairs have an increased thickness of  $3\lambda/4$  to achieve a better mechanical stability of the membrane. The reflection measurements show that the grown DBR has a center wavelength of 851 nm and a bandwidth of 23 nm (see fig. 12) in which the reflectivities keep higher than 99.7%. The penalty of making the layers thicker is a reduction of the bandwidth of 40 nm as compared to a mirror consisting of  $\lambda/4$ -thick layers only (calculated with matrix transfer method<sup>20</sup>).

## 5. CHARACTERISATION

### 5.1 Long wavelength VCSEL

For the preliminary static and dynamic device characteristics, a flat and non-tunable dielectric DBR is evaporated on the top of the half-VCSEL (same material composition for the bottom mirror consisting of 5 pairs). The measurements has been done at room temperature and at 80 °C.<sup>26</sup> Fig. 11 (b) shows the P-I-V characteristics of a long-wavelength VCSEL consisting of a 5.5  $\mu\text{m}$  BTJ. The single-mode fiber coupled optical output power at thermal roll-over shows a maximum value of 6.7 mW at room temperature and 3 mW at 80 °C. The threshold current amounts 1.2 mA and 2.1 mA for 20 °C and 80 °C, respectively. The voltage drop over the fully applied current range from 0 – 27 mA shows a kink voltage of approximately 0.9 V and a maximum value of 2.1 V. This current-voltage curve does not vary over the full considered temperature range from 20 °C to 80 °C. The SMSR exceeds 50 dB. Fig. 11 (a) shows thermal tuning of the wavelength, which is limited to a couple of nanometers. In order to determine the resonance frequency, a small signal modulation has been applied for various laser bias currents. Fig. 11 (c) presents the measured  $S_{21}$ -parameter plotted over the modulation frequency. As can be seen, a maximum 3 dB-cutoff frequency of 11 GHz is reached for bias currents smaller than the respective roll-over currents and is stable over the whole temperature range. This means that these devices can be applied for data transmission in the 12.5 GBit/s range for each desired and specified temperature within 20 °C and 80 °C. To realise a wide tunable laser one has to replace the evaporated top flat DBR by an external micro-electro-mechanical

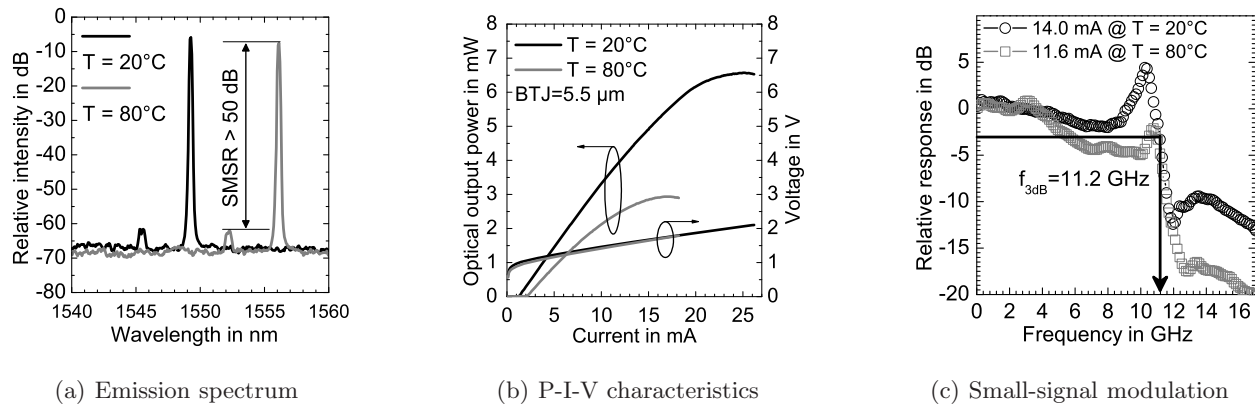


Figure 11. Measurement results for the 1550 nm VCSEL. All measurements have been done at room temperature (blue) and at 80 °C (red). A SMSR > 50 dB and a small signal modulation bandwidth of the laser current of  $\approx 11$  GHz has been achieved.

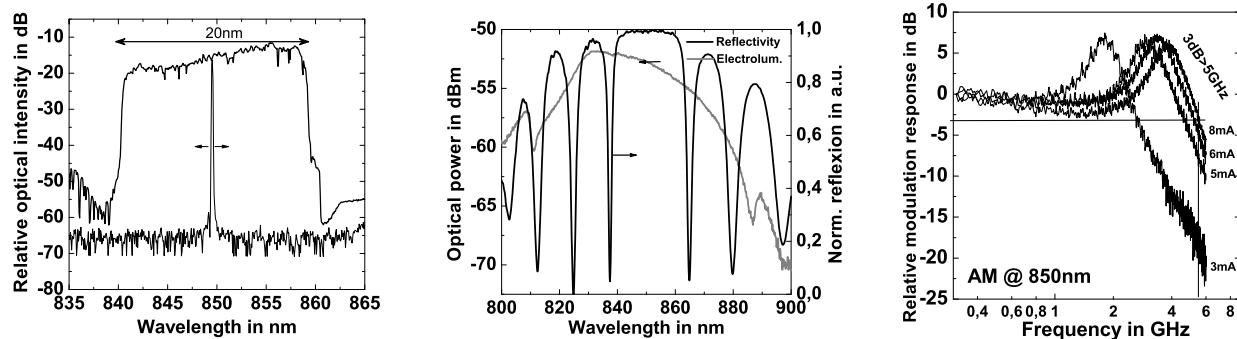
system (MEMS) mirror. The static and dynamic characteristics of the new generation MEMS-VCSEL based on BCB are under investigation.

## 5.2 Short wavelength VCSEL

To characterize the tunability of the short wavelength VCSEL, the optical emission spectrum of the device has been measured for different heating currents flowing through the movable membrane. Fig. 12 (a) shows the spectrum of the VCSEL during the actuation of the membrane at a constant laser current of 8 mA. A maximum tuning current of 12 mA is needed for tuning over the whole tuning range. A mode-hop free continuous single mode tuning of about 19 nm (from 840 nm to 859 nm) with a SMSR of about 40 dB throughout the tuning range has been achieved. A comparison of the electroluminescence of the half-VCSEL and the top-mirror stop-bandwidth, as it is shown in fig. 12 (b), shows that the limitation of the tuning range is caused by the bandwidth of the top mirror.<sup>17</sup> This shows up that there are still capacities to enlarge the tuning range using broadband series DBR. These can be made of dielectric materials providing much larger stop bandwidth as they have been used for the long wavelength VCSEL, already. The first tested devices had a maximum output power of 0.17 mW ( $-7.5$  dBm) and an electrical resistance of about 150  $\Omega$  at 8.3 mA thermal rollover at a center wavelength of 850 nm. This quite high serial resistance leads to a significant decrease of the optical output power due to electro-thermal heating. Optimisations of the device reduced the half-VCSEL resistance to 100  $\Omega$  resulting in an output power of 0.8 mW at 9.2 mA (thermal rollover). For determining the modulation bandwidth of the short wavelength VCSEL the small signal frequency response ( $S_{21}$ ) of the device has been measured using a fast photodetector connected to a network analyzer. The modulation response of the VCSEL at a constant wavelength of 850 nm for different laser bias currents 3, 5, 6, 8 mA is shown in Fig. 12 (c). A maximum 3 dB cut-off frequency of 5.5 GHz and a resonance frequency of 4 GHz have been achieved at the laser rollover current of 8 mA. Thus the devices already fulfill the high speed requirements (2.5 GBit/s) for optical interconnects.

## 6. CONCLUSION AND OUTLOOK

A two-chip concept for electro thermally tunable VCSEL in the 850 nm range has been demonstrated. The device shows an excellent SMSR ( $> 40$  dB) over the whole tuning range which cover the desired wavelength regions for optical interconnects. The given tunable VCSEL is capable for modulation frequencies  $> 5$  GHz. An output power of 1 mW is desirable for optical interconnects thus it needs to be further increased. Additionally, the polarisation stability during wavelength tuning as well as for AM of the laser current needs to be investigated. For both, the 850 nm as well as 1550 nm VCSEL the implementation of a sub wavelength grating is under investigation. Now, the devices need to be implemented with the tunable membranes for future measurements. A non tunable half-VCSEL capable for the integration with a movable mirror membrane has been completed



(a) Optical emission spectrum for a fixed tuning current and tuning envelope  
 (b) Electro luminescence spectrum and reflectivity bandwidth of the movable mirror membrane  
 (c) Small signal modulation

Figure 12. Measurement results for the 850 nm VCSEL. A mode hop free tuning over 20 nm and bandwidths up to 5 GHz are illustrated.

with a fixed top mirror for first investigations. A record output power of  $\approx 6$  mW at room temperature could be achieved. A high SMSR  $> 50$  dB and modulation speeds in the region of 10 GHz have been realized with the non tunable flat mirror. Devices not designed for high speed modulation showed a tuning range of 76 nm. Future investigations will focus on the high speed laser devices with a tunable mirror membrane. The given two-chip concept has the advantage to be able to separately optimize the fabrication processes of the membrane as well as the half-VCSEL chip. This enabled a rapid progress in developing tunable VCSEL. This concept is not capable for mass production and needs additional steps for the alignment of the membrane chip and the half-VCSEL and an additional waferbonding or gluing process of the two separate chips. That's why we are working on an integrated solution which is based on monolithical steps only. All the experience gained with the two-chip concept will be used to develop a new process capable for mass production. First integrated tunable VCSEL have already been developed for 850 nm.<sup>29</sup> New half-VCSEL which are capable for monolithical integration of the movable mirror membrane in the 1550 nm region are being processed.

## REFERENCES

1. O. Akanbi, "Bi-directional dense wavelength division multiplexed systems for broadband access networks", Ph.D. dissertation, School of Electrical and Computer Engineering, Georgia Institute of Technology, 12 2006.
2. ITU-T Recommendation G.692 (October 1998)
3. Clause 64, 65, IEEE 802.3ah standard, approved (24 June 2004)
4. ITU-T Recommendation G.984.2 (2003)
5. Pressrelease from LG Ericsson: "LG-Nortel Demonstrates Full WDM-PON Ecosystem at FTTH Council Europe 2010", 2010-02-24.
6. L. G. Kazovsky et al., "Next-generation optical access networks", J. Lightwave Technol., vol. 25, no. 11, pp. 3428-3442, Nov. 2007
7. J. Ingenhoff; , "Athermal AWG devices for WDM-PON architectures," Lasers and Electro-Optics Society, 2006. LEOS 2006. 19th Annual Meeting of the IEEE , vol., no., pp.26-27, Oct. 2006
8. Hofmann, W. et al., "1.55- $\mu$ m VCSEL Arrays for High-Bandwidth WDM-PONs," Photonics Technology Letters, IEEE , vol.20, no.4, pp.291-293, Feb.15, 2008
9. Artundo, I. et al., "Selective optical broadcast component for reconfigurable multiprocessor interconnects," IEEE Journal of Selected Topics in Quantum Electronics, vol.12, no.4, pp.828-837, July-Aug. 2006
10. Gordon E. Moore, "Cramming more components onto integrated circuits," Electronics, Volume 38, Number 8, April 19, 1965
11. Patel, R.R. et al., "Multiwavelength parallel optical interconnects for massively parallel processing," IEEE Journal of Selected Topics in Quantum Electronics, vol.9, no.2, pp. 657- 666, March-April 2003

12. W. H. Cheng et al., "Spectral characteristics for a fiber grating external cavity laser," *Optical and Quantum Electronics*, vol.32, no.3, pp. 339-348, March 2000.
13. Chang-Hasnain, C.J., "1.5-1.6  $\mu\text{m}$  VCSEL for metro WDM applications," 2001. IPRM. IEEE International Conference On Indium Phosphide and Related Materials, vol., no., pp.17-18, 2001
14. Tayebati, P. et al., "Half-symmetric cavity tunable microelectromechanical VCSEL with single spatial mode," *Photonics Technology Letters, IEEE* , vol.10, no.12, pp.1679-1681, Dec 1998
15. Jatta, S. et al., "Bulk-Micromachined VCSEL At 1.55  $\mu\text{m}$  With 76 nm Single-Mode Continuous Tuning Range," *Photonics Technology Letters, IEEE* , vol.21, no.24, pp.1822-1824, Dec.15, 2009
16. P. Meißner et al., "Micromachined two-chip WDM filters with stable half symmetric cavity and their system integration," *Electronic Components and Technology Conference, 2002. Proceedings. 52nd*
17. H. A. Davani et al., "Widely tunable high-speed bulk-micromachined short-wavelength MEMS-VCSEL" *IEEE Semiconductor Laser Conference 2010, ISLC 2010*, page 14-15.
18. P. Debernardi et al., "Modal Properties of Long-Wavelength Tunable MEMS-VCSELs With Curved Mirrors: Comparison of Experiment and Modeling," *IEEE Journal of Quantum Electronics*, vol.44, no.4, pp.391-399, April 2008
19. L. A. Coldren, S.W. Corzine, "Diode Lasers and Photonic Integrated Circuits", John Wiley & Sons, Inc., New York, 1995.
20. J. Chilwell, I. Hodgkinson. "Thin-film field-transfer matrix method of planar multilayer waveguides and reflection from prism-loaded waveguides", *J. Opt. Soc. Am. A1* (1984) 742-753
21. S. Healy et al., *IEEE J. of Quantum Electronics*, Vol. 46, No. 4, pp. 506-512, April 2010.
22. B. Kögel et al., "Long-wavelength MEMS tunable vertical-cavity surface-emitting lasers with high sidemode suppression" 2006 *J. Opt. A: Pure Appl. Opt.* 8 S370
23. B. Kögel et al., "Tuning Dynamics of Micromachined Surface-Emitting Lasers with Broadband Long-Wavelength Coverage," *Photonics in Switching, 2007* , vol., no., pp.111-112, 19-22 Aug. 2007
24. M. Müller et al., *IEEE Photonics Technology Letters*, 21, pp . 1615-1617, 2009
25. M. Maute et al., "MEMS Tunable 1.55  $\mu\text{m}$  VCSEL With Extended Tuning Range Incorporating a Buried Tunnel Junction", *IEEE Photonics Technology Letters*, vol. 18(5), pp. 688-690, 2006.
26. Tobias Gründl et al., "High-Speed and HighPower Vertical-Cavity Surface-Emitting Lasers based on InP suitable for Telecommunication and Gas Sensing", *SPIE Remote Sensing 2010*, Nr: 7828-6
27. M.-C. Amann and M. Ortsiefer, "Long-wavelength (1.3  $\mu\text{m}$ ) InGaAlAs-InP vertical-cavity surface-emitting lasers for applications in optical communications and sensing", *phys. stat. sol. (a)* 203 (14),pp. 3538-3544, 2006
28. Dissertation, Markus Maute, Walter Schottky Institut, Technische Universität München, "Mikromechanisch abstimmbare Laser-Dioden mit Vertikalresonator", Vol.81, ISBN 3-932749-81-2
29. B. Kögel. et al., "Integrated Tunable VCSELs With Simple MEMS Technology" *IEEE Semiconductor Laser Conference 2010, ISLC 2010*.